RSC Advances

PAPER

View Article Online
View Journal | View Issue

Cite this: *RSC Adv.*, 2023, **13**, 1236

Enhanced photoluminescence of potassium-doped tungsten oxide by acetone exposure†

Aman Patel,*[a] Weigang Lu,[a] Blake Birmingham,[a] Michael Johnson,[b] Danling Wang,[b] Zhenrong Zhang [a] and Kai Wang *[cd]

Received 5th October 2022
Accepted 19th December 2022

DOI: 10.1039/d2ra06267d

rsc.li/rsc-advances

Studies of optical properties of doped nanocrystals of tungsten trioxide can elucidate new information about the material. A novel molecule-enhanced photoluminescence (PL) of potassium-doped tungsten trioxide (K_xWO) was explored in the presence of different gases to understand charge transfer between molecules and K_xWO on the properties of the material. We performed Raman spectroscopy and PL experiments in the presence of gaseous acetone or ethanol mixed with other gases (N_2 and O_2). PL at 630 nm from K_xWO was observed and further enhanced when the sample was continuously irradiated with a 532 nm CW laser in acetone. A mechanism of strong emission of the PL induced by the charge transfer between the acetone and the K_xWO is proposed.

Introduction

Transition metal oxides are one of the most important and widely used solid materials. Tungsten oxide is one of the most common transition metal oxides that has been extensively studied. It has several different oxidation states including tungsten(III) oxide, tungsten(IV) dioxide, tungsten(VI) trioxide, and tungsten pentoxide.[1,2] They can form various heterogeneous nanocrystals, which have found applications in photoelectrochemistry,[3,4] photocatalysis,[5,6] photoelectrodes,[7,8] gas and humid sensing,[9,10] *etc*. Particularly, tungsten trioxide (WO_3) has multiple crystal phases, which are generated in different synthesis conditions and lead to various properties such as the ferroelectric effect,[11] electrochromic effect,[12,13] chemiresistive effect,[14] and so on. These properties are utilized to implement their applications. For example, WO_3 has received much attention due to its viable functioning as a photocatalyst with a response to visible light wavelengths.[15–17] The bandgap and defect states of WO_3 can be tuned by changing the oxygen vacancy concentration and doping with various elements including K, N, *etc*[13,18]. By tuning these properties, WO_3 can be modified for the appropriate applications. For example, K_xWO has shown a promising prospect for gas sensing just like other MWO (M: Metal). Doping potassium enables a large percentage of exposed (002) crystal facets, which has proven to show a selective response to acetone.[14] Further study of the bandgap structures and charge transfer mechanism of doped WO_3 can lead to the development of a low-cost and environmentally friendly photocatalyst and electrochromic devices.[16,19]

Photoluminescence (PL) spectroscopy has been used to explore band structures[20–22] and measure purity and crystalline quality. It can be employed to identify certain impurities and study defect states that result from doping and vacancies.[23] Optical techniques as a contact-free method can, therefore, be used to investigate charge carrier dynamics and photosensitive mechanism of these nanocrystals,[24] which are very important for practical applications, such as catalyst and gas sensing. Generally, when crystalline materials interact with particular molecules, their optical properties are changed. Optical measurements of materials in various gaseous environments have revealed new properties of the materials and information about the charge transfer mechanisms occurring inside the material. The charge transfer that happens during the interactions can enhance or quench the photoluminescence of the 2D materials (*e.g.*, $MoSe_2$ and MoS_2).[22,25] When monolayer MoS_2 was photo irradiated in O_2, the PL intensity of the MoS_2 flake edges increased, which was attributed to the charge transfer of the absorbed O_2.[25] The UV emission and conductivity of ZnO can be tuned by the adsorption of species that either donate or extract electrons from the conduction band.[22,25,26] Exposure of ZnO to an oxygen-rich environment drastically increased the green emission while decreasing the UV emission and conductivity of ZnO. When exposed to N_2, the green emission of ZnO was quenched while the UV emission was enhanced.

[a]*Department of Physics, Baylor University, Waco, 76798, Texas, USA. E-mail: aman_patel1@baylor.edu*

[b]*Department of Electrical and Computer Engineering, North Dakota State University, Fargo 58102, ND, USA*

[c]*School of Physics and Astronomy, Sun Yat-sen University, Zhuhai 519082, China. E-mail: wangk289@mail.sysu.edu.cn*

[d]*Center of Quantum Information Technology, Shenzhen Research Institute of Sun Yat-sen University, Nanshan Shenzhen 518087, China*

† Electronic supplementary information (ESI) available: Raman spectra acquired in ambient air, deconvolution of Raman spectra, the XRD spectra of NS-$K_{1.8}WO$ and S-$K_{1.8}WO$ nanorods after annealing, and UV-vis spectra of K_xWO. See DOI: https://doi.org/10.1039/d2ra06267d

Exposure of ZnO to water vapor increased the conductivity of the sample, without affecting the emission profile.[26]

Blue and red PL emissions have been observed in previous studies from WO_3 nanostructures.[12,13,27–30] The emission has been attributed to the presence of oxygen vacancies,[12,27] quantum confinement,[28] and the photonic band gap.[29] The PL optical properties of the WO_3 have also been studied for applications in electrochromic devices.[12,13] In general, the observed PL intensity has been weak. Utilizing the effect of different gaseous environments to alter the optical properties of WO_3 is a possible option that has yet to be explored. In addition, understanding the role of charge transfer on the optical properties of WO_3 in the molecule–oxide interaction would be important for its various applications.

In this paper, we used PL and Raman spectroscopies to study the interaction between newly synthesized nanomaterial $K_xW_7O_{22}$ (K_xWO) nanorods and gaseous acetone mixed with other gases (O_2 and N_2). The results show that the presence of acetone molecules induces a strong PL when using N_2 as the carrying gas, but it is much lower when K_xWO was exposed to ethanol. The results indicate the vital role of the charge transfer in the sensitive response of K_xWO to acetone. The acetone-enhanced PL provides new insights into designing nanomaterial's functionalities during the synthesizing process for various applications including photocatalysts, smart windows, and gas sensors such as acetone detectors.

Experimental methods

The samples of K_xWO nanorods used in the experiments were prepared from NEWS (Nano-Electronic Wearable Sensors) lab at North Dakota State University. K_xWO was synthesized using a hydrothermal method.[30–33] A precursor solution containing $Na_2WO_4 \cdot 2H_2O$ (95%, Alfa Aesar, Tewksbury, MA, USA), oxalic acid dehydrate (>99%, VWR, Radnor, PA, USA), K_2SO_4 (>99%, VWR, Radnor, PA, USA), and hydrochloric acid (36–38%, Aqua Solutions Inc., Deer Park, TX, USA) was first made. To synthesize surfactant-treated KWO (S-KWO), poly(ethylene glycol)-*block*-poly(propylene glycol)-*block*-poly(ethylene glycol) (designated PEG-PPG-PEG; Pluronic L-121, Sigma-Aldrich, St. Louis, MO, USA) was added to the precursor solution and stirred for 10 min. The solution was then put into a 30 mL autoclave for synthesis and heated at 225 °C for 24 h for hydrothermal growth. The hydrothermal product was then dried in an oven at 75 °C to form a powder. The powdered samples were post-annealed at 350 °C for 1 h. KWO is insoluble in water and ethanol.

The first sample of $K_{1.8}WO$ nanorods that was prepared without the use of Pluronic L-121 was designated as the NS-$K_{1.8}WO$, and the second sample of $K_{1.8}WO$ nanorods, which was prepared using the Pluronic L-121, was designated as the S-$K_{1.8}WO$ sample. As-synthesized KWO was dispersed in ethanol to form a suspension solution. This solution then was drop-casted onto on glass slides as thin films consisting of nanorods.

The thin film samples of NS-$K_{1.8}WO$ and S-$K_{1.8}WO$ were exposed to various gaseous environments in an *in situ* reaction cell (Linkam® Scientific THMS600). The reaction cell was placed on a lab-built Raman microscope setup to monitor the spectral changes in the Raman scattering and PL. A 5× objective lens was used to collect the spectra through a quartz viewpoint on the reaction cell in a Leica confocal microscopy. The spectra in the range 500–725 nm were recorded using a Princeton Instruments SCT-320 spectrometer. The grating of the spectrometer was 600 lines per mm. The setup consisted of a 532 nm continuous wave (CW) laser (Coherent Compass 532 Green DPSS Laser) and a 405 nm CW laser (Thor Labs L405P20 laser diode) as the pump laser for the Raman spectra and the PL spectra.

Before the samples were placed in the reaction cell, the cell was baked at 80 °C overnight to remove any residual chemicals. Multiple Raman and PL spectra were taken while nitrogen was flowing through the cell to acquire baseline spectra at room temperature. Experiments containing vapor from liquid (acetone, ethanol, and H_2O) were conducted using a saturator. Prior to the Raman and PL measurements, pure acetone/ethanol/H_2O vapor was bubbled into the cell for 30 minutes using either nitrogen or O_2 as the carrier gas. The flask used to store the liquid acetone or ethanol was heated using a hot plate at 56 °C and 78 °C, respectively. The vapor pressures of acetone and ethanol are 1 atm at these temperatures respectively. The flow rate of pure gases and gas-chemical mixers passing through the cell for each experiment was fixed at 40 mL min^{-1}.

Time-dependent PL and Raman measurements were taken from randomly chosen areas of the sample. The acquisition time was 0.5 seconds, and the laser power was 1 mW for the experiments using a 532 nm laser and a 405 nm laser. The experiment was performed at three uncorrelated areas on the sample to minimize the effect of the unavoidable non-uniform deposition of the $K_{1.8}WO$ nanorods. These areas were not exposed to a laser before the measurement to avoid the influence of the historical laser exposure. One representative data set is presented as the results from these three areas; it shows uniform characteristics, although the absolute signal intensities depend on the amount of $K_{1.8}WO$ nanorods in the laser spot. The Raman shift was calibrated using a silicon sample.

Results

The XRD spectra show that the crystal structure of both NS-$K_{1.8}WO$ and S-$K_{1.8}WO$ is of hexagonal tungsten trioxide (*h*-WO_3) (Fig. 1a).[34] The sample grown with surfactant (S-$K_{1.8}WO$) shows a higher ratio of (001) facet to (200). Both S-$K_{1.8}WO$ and NS-$K_{1.8}WO$ samples are ensembles of nanorods (Fig. 1b and c). The length of the nanorods in S-$K_{1.8}WO$ is around 30–60 nm with an aspect ratio of 2 – 3. The length of the nanorods in NS-$K_{1.8}WO$ is around 30–100 nm with an aspect ratio of 2 – 6. Raman spectra were also taken on these $K_{1.8}WO$ samples to examine the crystal structure of the samples. Raman spectroscopy is sensitive to the crystal structure and phase transition as it measures the vibrational modes of a crystal lattice. The black spectra in Fig. 2 show the Raman spectra acquired in pure nitrogen in the Linkam cell on samples S-$K_{1.8}WO$ and NS-$K_{1.8}WO$ with the 532 nm laser. The spectra acquired in nitrogen are the same as those in ambient air (Fig. S1†). The spectra show that S-$K_{1.8}WO$ consists of the *h*-

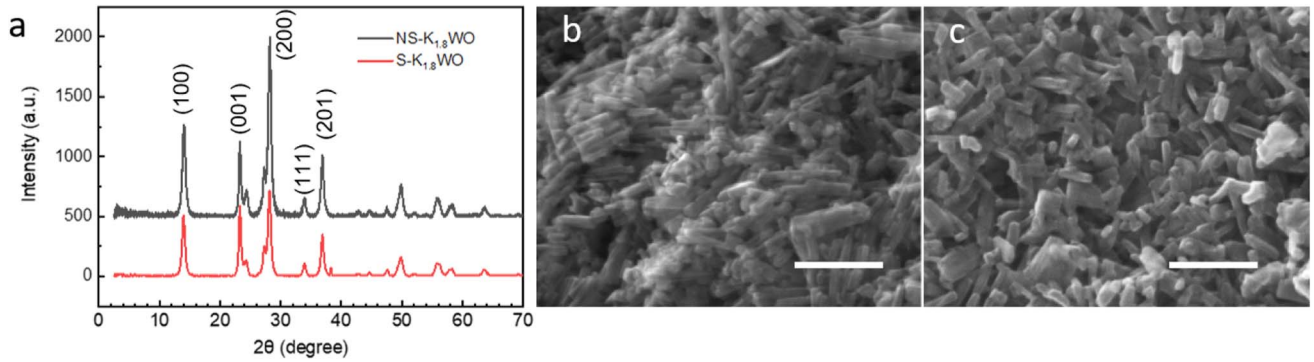

Fig. 1 $K_{1.8}WO$ sample characterizations. (a) The XRD spectra of NS-$K_{1.8}WO$ and S-$K_{1.8}WO$ nanorods. SEM images of (b) NS-$K_{1.8}WO$ and (c) S-$K_{1.8}WO$ nanorods. The scale bar is 1 μm. The X-ray diffraction (XRD) patterns of the KWO were collected with a Siemens D5000 diffractometer in $\theta-2\theta$ mode using Cu Kα radiation ($\lambda = 1.5406$ Å) as the X-ray source (operated at 40 kV and 30 A). The scanning step size for XRD was 0.05°. Scanning electron microscope (SEM) images were acquired with a FEI Focused Ion Beam SEM Microscope (FEI-Versa 3D) operated at 30 kV.

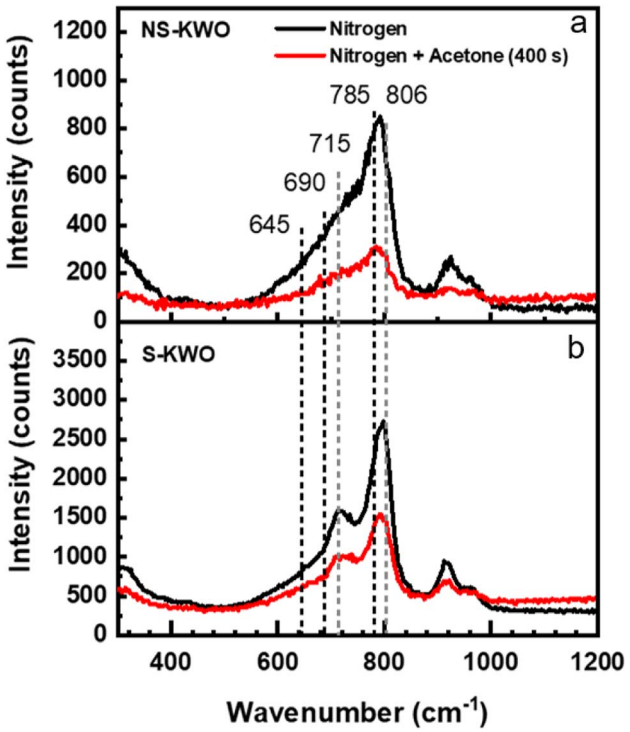

Fig. 2 Raman spectra of $K_{1.8}WO$ nanorod samples with the 532 nm laser excitation. Spectra in black are obtained on (a) NS-$K_{1.8}WO$ and (b) S-$K_{1.8}WO$ when the sample is in nitrogen. Spectra in red are obtained after the samples were exposed to the laser for 400 seconds in an acetone-saturated environment.

phase of WO_3 (Fig. 2b), which is identified by Raman shifts at 788, 690, and 645 cm^{-1}.[22] In theory, the main characteristic Raman vibrational modes of *h*-WO_3 are at 817, 690, and 645 cm^{-1}, which result from the O–W–O stretching.[22] Experimentally, the 691 cm^{-1} is consistently observed for *h*-WO_3.[22] However, the 817 cm^{-1} has only been observed in some of the *h*-WO_3 particles depending on the preparation condition of the samples.[22,35] Additionally, the peak at ~785 m^{-1} has been consistently observed for *h*-WO_3 [25] as well. This peak has been assigned to O–W–O stretching and it has been suggested to relate to oxygen vacancy.[35] The other Raman shifts show different phases and some unknown contributions. For example, the Raman shifts at 715 and 806 cm^{-1} correspond to the γ phase.[25,26,32,35] This indicates that the sample has the contribution from the γ phase although it is not obvious in the XRD spectra. The Raman shifts at 915 cm^{-1} and 950 cm^{-1} are observed in both samples. They suggest the contribution of the oxide hydrates.[36–38] These peaks have been attributed to the terminal W=O bonds.[36] For the sample (NS-$K_{1.8}WO$) grown without surfactant, no changes are clearly observed for the peaks that correspond to the *h*-phase (785, 690, and 645 cm^{-1}) and the contribution from the γ phase (806 cm^{-1} and 715 cm^{-1}) are less visible. The peak at 715 cm^{-1} shifted towards 730 cm^{-1}. It could be an indication of the phase transition that disrupts the O–W–O bonds.

To test the effect of acetone, the $K_{1.8}WO$ samples were exposed to acetone and nitrogen in the Linkam cell, and PL and Raman spectra were acquired by irradiating the samples with the 405 nm and 532 nm laser, respectively. The red spectra in Fig. 2 describe the Raman signal acquired in the mixture of acetone and nitrogen using a 532 nm laser. The intensities of the Raman shifts are lower than those in nitrogen. But the spectra consist of the same signatures as those in nitrogen for the respective samples. This implies that the acetone does not affect the phases of $K_{1.8}WO$ nanorods as expected. The reduction in intensity is most likely due to increased laser scattering in the beam path as acetone condensed on the quartz window of the Linkam cell.

There was no PL emission observed when the samples were irradiated by a 532 nm laser in pure nitrogen (Fig. 3a and c, black lines). The spectra obtained in the air show the same observation. The bandgap of the $K_{1.8}WO$ nanomaterial was experimentally measured to be ~2.9 eV (~430 nm) using ultraviolet-visible spectroscopy (Fig. S3†). Therefore, it is expected that the 532 nm photons do not have enough energy to directly excite the electrons from the valence band to the conduction band of $K_{1.8}WO$ in the single-photon excitation. However, when the samples were exposed to a saturated acetone

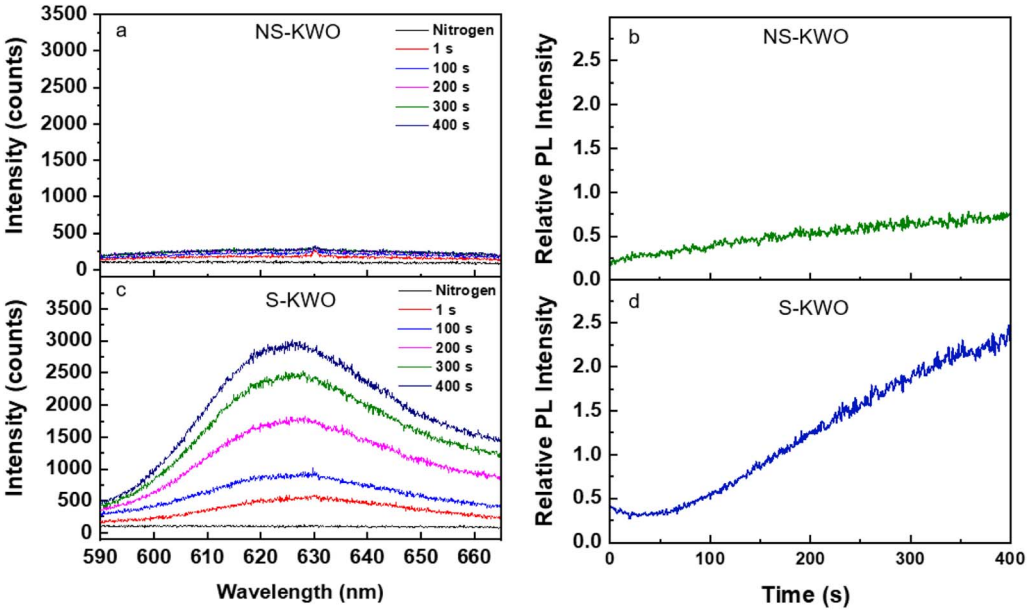

Fig. 3 (a) and (c) Temporal response of photoluminescence signal of the NS-$K_{1.8}$WO and S-$K_{1.8}$WO samples in acetone excited by a 532 nm laser. (b) and (d) Temporal trend of photoluminescence peak intensity relative to the peak intensity of the Raman signal for samples in acetone.

environment in the reaction cell and radiated with a 532 nm laser, a PL signal emerged from both S-$K_{1.8}$WO and NS-$K_{1.8}$WO samples, centered at 630 nm (Fig. 3a and c). The PL intensity of S-$K_{1.8}$WO is much stronger than that of NS-$K_{1.8}$WO.

To quantify the comparison of the PL intensity, we use the relative intensity, which is defined as the ratio of the peak intensity of the PL signal and the peak intensity of the Raman shift at ~795 cm^{-1} from the spectrum that was taken in the same scan. This removes intensity variation due to the effect of the non-uniform deposition of the $K_{1.8}$WO nanorods in the thin film samples. The intensity of the PL signal increased with continuous laser radiation (Fig. 3b and d) for both NS-$K_{1.8}$WO and S-$K_{1.8}$WO samples. It was also observed that the relative PL intensity for sample S-$K_{1.8}$WO increased 3 times faster than that of the sample NS-$K_{1.8}$WO. Moreover, a blank experiment in the absence of the KWO material was conducted on a glass substrate in acetone vapor in Linkam cell excited using a 532 nm laser. There is no fluorescence observed without KWO (Fig. S4†) which confirms that the PL was from the interaction between acetone and KWO and not from gaseous acetone.[39,40]

To understand the origin of the PL, the S-$K_{1.8}$WO sample was radiated with a 405 nm laser with the photon energy (3.1 eV), larger than the bandgap (~2.9 eV). Only weak PL peaks at 630 nm were observed in the presence of nitrogen (Fig. 4 top) or air. The intensity of the PL observed in a saturated acetone environment with nitrogen as the carrier gas (Fig. 4 bottom) is comparable to that observed in pure nitrogen. The PL intensity remained constant with extended 405 nm laser irradiation. No increase in the PL intensity was observed when the S-$K_{1.8}$WO sample was exposed to acetone. Weak PL peaks are consistent with what is reported in other doped WO_3 using UV irradiation.[12]

To test the recovery time of the intensive PL signal of the $K_{1.8}$WO nanorods in the presence of acetone, spectra were continuously acquired from one spatial location on the sample

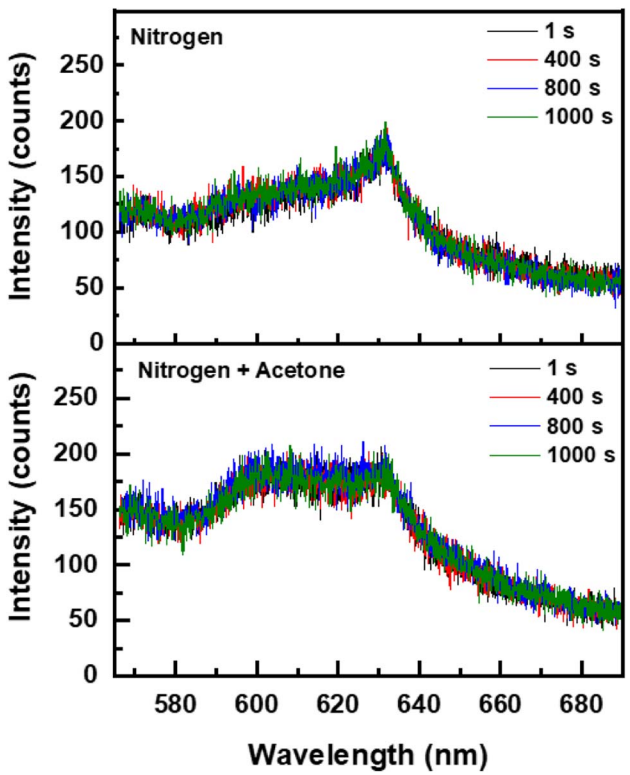

Fig. 4 Temporal response of photoluminescence signal of the S-$K_{1.8}$WO sample excited by a 405 nm laser in (Top) nitrogen and in (Bottom) acetone and nitrogen, respectively.

when the 532 nm laser beam was blocked for small intervals of time. The PL intensity increased monotonically in the first 400 s and went to zero when the laser path was blocked (Fig. 5). Once the laser was irradiated again, the PL went almost immediately back to the intensity before the laser was off. However, the longer the sample was not radiated, the longer it took for the PL to recover. The PL signal required 5 seconds, 9 seconds, and 13 seconds to go from zero to plateau when the sample was not radiated for 40 seconds, 90 seconds, and 120 seconds, respectively. This result indicates that the accumulated irradiation in acetone by the laser is needed to observe the strong PL signal.

To test the role of acetone in the observed PL emission, additional experiments were conducted in various pure gases such as nitrogen, water vapor, and oxygen respectively with the irradiation of 532 nm laser. We used the sample S-$K_{1.8}WO$ to monitor the behavior as the sample displayed better sensitivity to the environment than sample NS-$K_{1.8}WO$ (Fig. 3). There was no PL signal observed on the S-$K_{1.8}WO$ sample in the presence of pure water, nitrogen, and oxygen gas (Fig. 6). Moreover, a mixture of gases such as ethanol with nitrogen, acetone with nitrogen, and acetone with oxygen separately were also tested using a 532 nm laser. The PL signal was observed in the presence of ethanol with nitrogen, acetone with nitrogen, and acetone with oxygen. The strongest PL signal was observed in the presence of acetone with nitrogen as the carrier gas.

To quantitatively compare the effect of the various gases on the PL of $K_{1.8}WO$, the ratio of the PL signal intensity observed after 400 seconds of laser exposure to the intensity of Raman shift at ~795 cm^{-1} taken from the same scan was used. The intensity of the PL signal acquired from the S-$K_{1.8}WO$ sample in the mixture of nitrogen and ethanol was only 17% of that of the S-$K_{1.8}WO$ sample in the presence of acetone with nitrogen. It is known that the charge-carrier density affects the line shapes and positions of the PL peaks.[22,25] This implies that the charge transfer from the acetone to $K_{1.8}WO$ nanomaterials is critical for the PL signal. The lone electron pair on the oxygen atom in acetone acts as the electron donor. Among the various molecules tested, the positive inductive effect of alkyl groups has the order of $C(CH_3)_3 > CH(CH_3)_2 > CH_2CH_3 > CH_3 > H$. The positive inductive effect of $C(CH_3)_3$ makes acetone a good electron donor with a large dipole moment. Therefore, ethanol introduces lower PL intensity than acetone does, and H_2O introduces no PL. When the carrier gas changes from inert N_2 to O_2, even though acetone was used for both experiments, the relative intensity of the PL signal was significantly lower. This could be because oxygen is more electronegative or a stronger electron accepter than nitrogen. Oxygen takes electrons away from the $K_{1.8}WO$ sample, which is why the PL intensity is significantly lower.

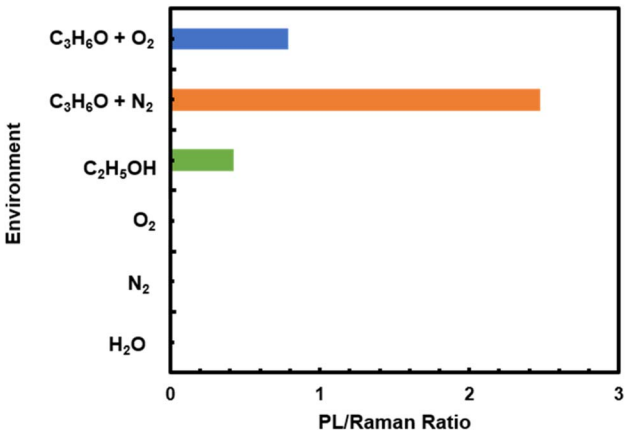

Fig. 6 The maximum relative photoluminescence signal intensity observed after 400 seconds of laser exposure on the sample S-$K_{1.8}WO$ in a saturated environment of each gas or gas mixer.

Discussion

The wavelength dependence of the PL suggests the presence of defect states in the bandgap of $K_{1.8}WO$ (Fig. 7). $K_{1.8}WO$ is a p-type semiconductor,[32,41] which has an electron acceptor energy level near the valence band (Fig. 7). The experimental bandgap of the $K_{1.8}WO$ samples is ~2.9 eV (430 nm). The photons from

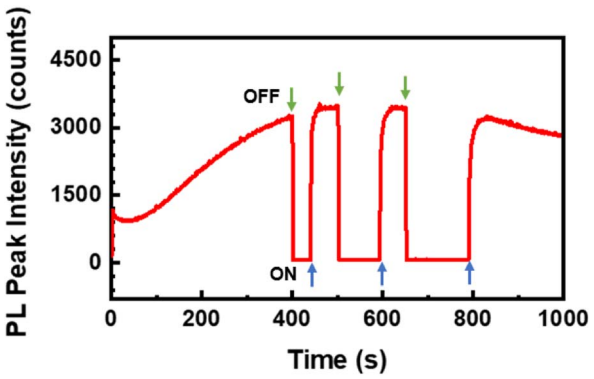

Fig. 5 Temporal trend of the peak intensity of the photoluminescence signal from the sample S-$K_{1.8}WO$ in the presence of acetone. The gaps at 400 seconds, 500 seconds, and 650 seconds represent the time interval for which the laser beam was blocked.

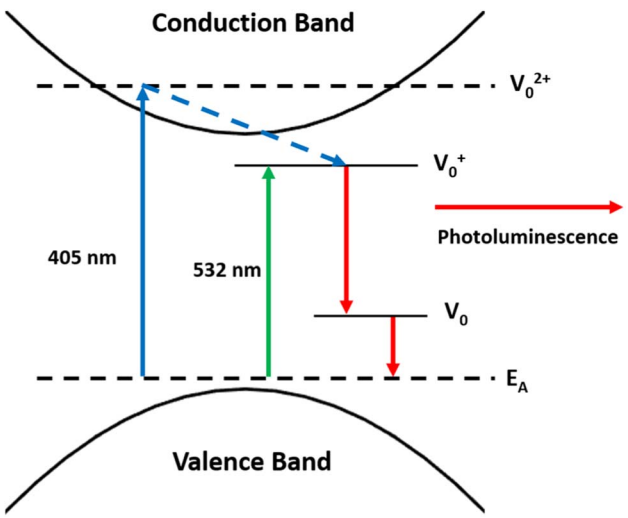

Fig. 7 Bandgap structure of $K_{1.8}WO$ with oxygen vacancies.

the 405 nm laser can excite electrons from the valence band/acceptor state to the conduction band, which is why the PL signal (although not strong) was observed from the sample irradiated in the air or pure nitrogen (Fig. 4). However, PL was not observed in the air or pure nitrogen when using 532 nm laser for excitation (Fig. 3). This could be because the 532 nm photon is far off-resonant from the bandgap.

The PL of the $K_{1.8}WO$ samples dramatically changed when the sample was excited by a 532 nm laser in the presence of acetone. An enhanced PL signal was observed from both NS-$K_{1.8}WO$ and S-$K_{1.8}WO$ samples in the presence of acetone with nitrogen (Fig. 3). We attribute this to a charge transfer from acetone to $K_{1.8}WO$. This charge transfer can reduce static screening in the p-type semi-conductor and increase the probability of excitation of electrons from the valence band/acceptor states and, in turn, the probability of relaxation with a radiative emission. The photons with an energy of 2.33 eV (532 nm) have little probability of exciting the electrons to the conduction band in $K_{1.8}WO$, hence observed enhanced luminescence emission involves the energy states lying inside the bandgap. We propose that electrons might be excited to the defect states. The PL signal acquired from the K_xWO sample is most likely due to the emission of photons when the trapped electrons relax from the defect state to the electron acceptor level (Fig. 7).[12,42,43] The theoretical calculations show that doping of alkali metals does not introduce defect states in the bandgap.[18] Therefore, these defect states are most likely due to the oxygen vacancies,[12,44–47] as in other metal oxides nanomaterials.[26,45] It is known that these defect states can trap electrons. Similar PL emission in the visible region (~620 nm) was observed from WO_3 nanopowder and WO_{3-x} films with different polymorphs (orthorhombic and monoclinic structures) and phases in previous reports.[12,46] The emission was attributed to the optical transitions from oxygen vacancy states to the conduction band. Such a mechanism and bandgap structure were proposed in other defect-related luminescence in oxides.[48–50] However, such a strong gas-enhanced PL signal from oxides has not been observed before.

In principle, the emission at the same wavelength (630 nm) should exhibit when the sample is excited by the 405 nm laser. The excited electrons relax from the conduction band to the defect states, and subsequent relaxation to the electron acceptor level emits light at 630 nm (Fig. 7). The observed weak PL emission at 630 nm in Fig. 3 further supports the proposed optical transition from the defect state to the accepter level.

We also observed that the PL signal from the S-$K_{1.8}WO$ was strongly modulated if excited by the 532 nm laser and was less influenced while excited by 405 nm in the presence of acetone with nitrogen. This suggests that the energy difference between the accepting energy level and the defect states in $K_{1.8}WO$ is nearly in resonance with the 532 nm laser. Therefore, the intensity of the PL is significantly higher than the PL signal from the off-resonant excitation with the 405 nm laser. We speculate that acetone contributes to the enhanced PL in two processes. One is the direct adsorption of the acetone molecules at the defects sites which transfers the charge to the defect states.[51] The other is the oxidation of acetone *via* holes which reduces the static screening in the photoexcitation process.[46] The time scale of photoreaction (hundreds of seconds)[52,53] supports the involvement of photoreaction of acetone in the slow (hundreds of seconds) increase of the PL intensity. The increased PL recovery time when the laser was blocked by various time intervals (Fig. 5) also suggests the critical role of photoreaction in the enhancement of the PL signal. The longer the sample was not radiated, the longer it took to accumulate the charge density needed for the PL to recover *via* charge transfer. Ethanol molecules have a less electron-donating effect than acetone molecules; therefore, ethanol introduces lower PL intensity than acetone does. In addition, the KWO sample surface was covered by hydroxyl groups which were introduced during the film preparation process. Additional water is expected to have little charge transfer. When using O_2 as carrying gas, physisorbed and chemisorbed oxygen molecules could directly interact with $K_{1.8}WO$. The scavenging nature of O_2 would drain the charge from the sample. Therefore, the PL intensity is lower than that using N_2 as carrying gas (Fig. 6). This is because O_2 is more electron negative than N_2. Furthermore, the difference in the PL intensity between the NS-$K_{1.8}WO$ and S-$K_{1.8}WO$ suggests that the S-$K_{1.8}WO$ nanoparticles are more reactive toward acetone and more effective in extracting electrons from the acetone molecules. This could be due to a combination of the crystal structure and the exposed (002) crystalline facets. S-$K_{1.8}WO$ exhibits more γ phase (Fig. 2) and more (002) facets (Fig. 1).

Conclusions

Acetone-enhanced PL of a potassium-doped tungsten oxide nanomaterial at room temperature was studied using Raman spectroscopy and PL spectroscopy. An intensive PL signal was observed from the $K_{1.8}WO$ sample when it was irradiated with a 532 nm laser in the presence of acetone with nitrogen, acetone with oxygen, or ethanol with oxygen, respectively. The PL has several properties: (1) it was most sensitive to the presence of acetone with nitrogen; (2) the PL intensity of the S-$K_{1.8}WO$ sample treated with surfactant (Pluronic L121) was more sensitive to the presence of acetone than the NS-$K_{1.8}WO$ sample not treated with the surfactant; and (3) the sensitivity of the PL signal was higher with irradiation of the sample with the 532 nm laser than with the 405 nm laser. The data indicates that the band structure of potassium-doped tungsten oxide contains defect states in the bandgap. Our experiments reveal that the presence of acetone promotes the near resonant radiative emission when a $K_{1.8}WO$ sample is excited by a 532 nm laser. The charge transfer from acetone to S-$K_{1.8}WO$ during the photoirradiation is the key effect in enhancing the PL intensity of the potassium-doped tungsten oxide. K_xWO has found applications in gas sensing and furthermore, it would be a promising visible-light photocatalyst because of the strong molecule–material interaction. Due to the intense molecule-enhanced PL signal, potassium-doped tungsten oxide could also find its application in light-emitting optoelectronic devices. In addition, chemical doping could potentially introduce a new approach for tuning the color of the tungsten oxide materials

for the electrochromic smart windows. It is worth mentioning that if potassium is replaced by other alkali metals, the band gap of MWO (M: Metals) is modified but morphology and structure are similar.[54] They showed similar acetone sensing properties but PL might be similar to that of KWO as we observed.

Author contributions

Z. Z., K. W., and D. W. conceived and designed the project. M. J. synthesized samples. B. B built the Raman microscopy and high-pressure experimental setup and participated in the measurements. A. P. and W. L performed measurements and analyzed data. A. P. drafted the paper. Z. Z., K. W., and D. W. supervised the project. All authors discussed the results and commented on the manuscript.

Conflicts of interest

There are no conflicts to declare.

Acknowledgements

This work was partially supported by the National Science Foundation under Grants CHE-1905043, IIP-1941100, and the Office of Vice Provost for Research of Baylor University. Acknowledgment is made to the Donors of the American Chemical Society Petroleum Research Fund for partial support of this research. M. J. and D. W acknowledge support from NSF RII Track 2 FEC: OIA 2218046, NSF Eager-2226202 and ND EPSCoR Research funds. K. W. acknowledges support from the National Natural Science Foundation of China under grant 12174459 and the Shenzhen Science and Technology Program (2021Szvup172).

References

1 H. Zheng, J. Z. Ou, M. S. Strano, R. B. Kaner, A. Mitchell and K. Kalantar-zadeh, Nanostructured Tungsten Oxide – Properties, Synthesis, and Applications, *Adv. Funct. Mater.*, 2011, **21**, 2175–2196.

2 M. Wakizaka, W. J. Chun, T. Imaoka and K. Yamamoto, Multiple-Oxidation-State Tungsten-Oxide Clusters on a Carbon Surface as an Intersection between Molecular and Bulk Oxides, *Eur. J. Inorg. Chem.*, 2021, 1111–1116.

3 S. Xinjian, C. Lili, C. Il Yong, M. Ming, Z. Kan, Z. Jiheng, K. Jung Kyu, K. Jong Kyu, Z. Xiaolin and P. Jong Hyeok, Epitaxial growth of WO_3 nanoneedles achieved using a facile flame surface treatment process engineering of hole transport and water oxidation reactivity, *J. Mater. Chem. A*, 2018, **6**, 19542–19546.

4 G. Zheng, J. Wang, H. Liu, V. Murugadoss, G. Zu, H. Che, C. Lai, H. Li, T. Ding, Q. Gao and Z. Guo, Tungsten oxide nanostructures and nanocomposites for photoelectrochemical water splitting, *Nanoscale*, 2019, **11**, 18968–18994.

5 Z.-F. Huang, J. Song, L. Pan, X. Zhang, L. Wang and J.-J. Zou, Tungsten Oxides for Photocatalysis, Electrochemistry, and Phototherapy, *Adv. Mater.*, 2015, **27**, 5309–5327.

6 D. Xu, T. Jiang, D. Wang, L. Chen, L. Zhang, Z. Fu, L. Wang and T. Xie, pH-Dependent Assembly of Tungsten Oxide Three-Dimensional Architectures and Their Application in Photocatalysis, *ACS Appl. Mater. Interfaces*, 2014, **6**, 9321–9327.

7 F. Amano, M. Tian, G. Wu, B. Ohtani and A. Chen, Facile Preparation of Platelike Tungsten Oxide Thin Film Electrodes with High Photoelectrode Activity, *ACS Appl. Mater. Interfaces*, 2011, **3**, 4047–4052.

8 J. Bingjun, J. Eunji, M. Ming, K. Sungsoon, Z. Kan, K. Jin Il, S. Yongkeun and P. Jong Hyeok, Solution-processed yolk–shell-shaped $WO_3/BiVO_4$ heterojunction photoelectrodes for efficient solar water splitting, *J. Mater. Chem. A*, 2018, **6**, 2585–2592.

9 J. Li, X. Liu, J. Cui and J. Sun, Hydrothermal synthesis of self-assembled hierarchical tungsten oxides hollow spheres and their gas sensing properties, *ACS Appl. Mater. Interfaces*, 2015, **7**, 10108–10114.

10 P. Li, Z. Zhang, Z. Zhuang, J. Guo, Z. Fang, S. L. Fereja and W. Chen, Pd-Doping-Induced Oxygen Vacancies in One-Dimensional Tungsten Oxide Nanowires for Enhanced Acetone Gas Sensing, *Anal. Chem.*, 2021, **93**, 7465–7472.

11 P. M. Woodward, A. W. Sleight and T. Vogt, Ferroelectric Tungsten Trioxide, *J. Solid State Chem.*, 1997, **131**, 9–17.

12 P. Kaur, S. Kaur, D. Arora, K. Asokan and D. P. Singh, Influence of defect structure on colour tunability and magneto optical behaviour of WO_3 nanoforms, *RSC Adv.*, 2019, **9**, 20536–20548.

13 Y. Li, Z. Tang, J. Zhang and Z. Zhang, Defect Engineering of Air-Treated WO_3 and Its Enhanced Visible-Light-Driven Photocatalytic and Electrochemical Performance, *J. Phys. Chem. C*, 2016, **120**, 9750–9763.

14 M. Johnson, Q. Zhang and D. Wang, Room-temperature ferroelectric $K_2W_7O_{22}$ (KWO) nanorods as a sensor material for the detection of acetone, *Med. Devices Sens.*, 2019, **2**, e10044.

15 T. Mano, S. Nishimoto, Y. Kameshima and M. Miyake, Water treatment efficacy of various metal oxide semiconductors for photocatalytic ozonation under UV and visible light irradiation, *Chem. Eng. J.*, 2015, **264**, 221–229.

16 S. Nishimoto, T. Mano, Y. Kameshima and M. Miyake, Photocatalytic water treatment over WO_3 under visible light irradiation combined with ozonation, *Chem. Phys. Lett.*, 2010, **500**, 86–89.

17 V. Dutta, S. Sharma, P. Raizada, V. K. Thakur, A. A. P. Khan, V. Saini, A. M. Asiri and P. Singh, An overview on WO_3 based photocatalyst for environmental remediation, *J. Environ. Chem. Eng.*, 2021, **9**, 105018.

18 S. Tosoni, C. Di Valentin and G. Pacchioni, Effect of Alkali Metals Interstitial Doping on Structural and Electronic Properties of WO_3, *J. Phys. Chem. C*, 2014, **118**, 3000–3006.

19 V. T. Quyen, J. Kim, P.-M. Park, P. T. Huong, N. M. Viet and P. Q. Thang, Enhanced the visible light photocatalytic

decomposition of antibiotic pollutant in wastewater by using Cu doped WO_3, *J. Environ. Chem. Eng.*, 2021, **9**, 104737.
20 M. R. Hossain, O. Ama, Q. Zhang, M. Johnson and D. Wang, Investigation of Different Materials as Acetone Sensors for Application in Type-1 Diabetes Diagnosis, *Biomed. J. Sci. Technol. Res.*, 2019, **14**, 10940–10945.
21 G. Sakai, N. Matsunaga, K. Shimanoe and N. Yamazoe, Theory of gas-diffusion controlled sensitivity for thin film semiconductor gas sensor, *Sens. Actuators, B*, 2001, **80**, 125–131.
22 H.-V. Han, A.-Y. Lu, L.-S. Lu, J.-K. Huang, H. Li, C.-L. Hsu, Y.-C. Lin, M.-H. Chiu, K. Suenaga, C.-W. Chu, H.-C. Kuo, W.-H. Chang, L.-J. Li and Y. Shi, Photoluminescence Enhancement and Structure Repairing of Monolayer $MoSe_2$ by Hydrohalic Acid Treatment, *ACS nano*, 2016, **10**, 1454–1461.
23 O. Nobuto, M. Akiyo, N. Shin-ichi, J. Junjun, I. Yoshinori, K. Hidefumi and S. Yuzo, Visible-light active thin-film WO_3 photocatalyst with controlled high-rate deposition by low-damage reactive-gas-flow sputtering, *APL Mater.*, 2015, **3**, 104407.
24 N. Huo, S. Yang, Z. Wei and J. Li, Synthesis of WO_3 nanostructures and their ultraviolet photoresponse properties, *J. Mater. Chem. C*, 2013, **1**, 3999.
25 B. Birmingham, J. Yuan, M. Filez, D. Fu, J. Hu, J. Lou, M. O. Scully, B. M. Weckhuysen and Z. Zhang, Spatially-Resolved Photoluminescence of Monolayer MoS_2 under Controlled Environment for Ambient Optoelectronic Applications, *ACS Appl. Nano Mater.*, 2018, **1**, 6226–6235.
26 J. A. Röhr, J. Sá and S. J. Konezny, The role of adsorbates in the green emission and conductivity of zinc oxide, *Commun. Chem.*, 2019, **2**, 52.
27 M. Feng, A. L. Pan, H. R. Zhang, Z. A. Li, F. Liu, H. W. Liu, D. X. Shi, B. S. Zou and H. J. Gao, Strong photoluminescence of nanostructured crystalline tungsten oxide thin films, *Appl. Phys. Lett.*, 2005, **86**, 141901–141903.
28 T. Takagahara and K. Takeda, Theory of the quantum confinement effect on excitons in quantum dots indirect-gap material, *Phys. Rev. B: Condens. Matter Mater. Phys.*, 1992, **46**, 15578–15581.
29 J. Ruan, Z. Yang, A. Huang, Z. Chai, J. Qiu and Z. Song, Red photoluminescent property and modification of WO_3:Eu^{3+} inverse opal for blue light converted LEDs, *Opt. Mater.*, 2018, **75**, 224–229.
30 B. B. Wang, X. X. Zhong, C. L. He, B. Zhang, U. Cvelbar and K. Ostrikov, Solvent-dependent structures and photoluminescence of WO_{3-x} nanomaterials grown in nonaqueous solutions, *J. Alloys Compd.*, 2021, **854**, 1.
31 M. Yoshimura and K. Byrappa, Hydrothermal processing of materials: past, present and future, *J. Mater. Sci.*, 2007, **43**, 2085–2103.
32 D. Wang, Q. Zhang, M. R. Hossain and M. Johnson, High Sensitive Breath Sensor Based on Nanostructured $K_2W_7O_{22}$ for Detection of Type 1 Diabetes, *IEEE Sens. J.*, 2018, **18**, 4399–4404.
33 M. E. Johnson, Q. Zhang and D. Wang, KxWO Is a Novel Ferroelectric Nanomaterial for Application as a Room Temperature Acetone Sensor, *Nanomaterials*, 2020, **10**, 225.
34 XRD JCPDS Card No-752187.
35 A. Staerz, U. Weimar and N. Barsan, Understanding the Potential of WO_3 Based Sensors for Breath Analysis, *Sensors*, 2016, **16**, 1815.
36 L. Wang, A. Teleki, S. E. Pratsinis and P. I. Gouma, Ferroelectric WO_3 Nanoparticles for Acetone Selective Detection, *Chem. Mater.*, 2008, **20**, 4794–4796.
37 M. F. Daniel, B. Desbat, J. C. Lassegues, B. Gerand and M. Figlarz, Infrared and Raman study of WO_3 tungsten trioxides and WO_3, xH_2O tungsten trioxide tydrates, *J. Solid State Chem.*, 1987, **67**, 235–247.
38 Y. Li, Z. Tang, J. Zhang and Z. Zhang, Exposed facet and crystal phase tuning of hierarchical tungsten oxide nanostructures and their enhanced visible-light-driven photocatalytic performance, *CrystEngComm*, 2015, **17**, 9102–9110.
39 G. H. Damon, Fluorescence of Gaseous Acetone as a Test for Traces of Oxygen, Industrial & engineering chemistry, *Anal. Ed.*, 1935, **7**, 133–134.
40 S. Lind, J. Trost, L. Zigan, A. Leipertz and S. Will, Application of the tracer combination TEA/acetone for multi-parameter laser-induced fluorescence measurements in IC engines with exhaust gas recirculation, *Proc. Combust. Inst.*, 2015, **35**, 3783–3791.
41 M. Hossain, Q. Zhang, M. Johnson and D. Wang, Highly Sensitive Room-Temperature Sensor Based on Nanostructured $K_2W_7O_{22}$ for Application in the Non-Invasive Diagnosis of Diabetes, *Sensors*, 2018, **18**, 3703.
42 R. Salh, *Silicon nanocluster in silicon dioxide: Cathodoluminescence, energy dispersive X-ray analysis, infrared spectroscopy studies, Crystalline Silicon-Properties and Uses*, 2011, pp. 173–218.
43 C. Spindler, T. Galvani, L. Wirtz, G. Rey and S. Siebentritt, Excitation-intensity dependence of shallow and deep-level photoluminescence transitions in semiconductors, *J. Appl. Phys.*, 2019, **126**, 175703.
44 M. Gerosa, C. Di Valentin, G. Onida, C. E. Bottani and G. Pacchioni, Anisotropic Effects of Oxygen Vacancies on Electrochromic Properties and Conductivity of γ-Monoclinic WO_3, *J. Phys. Chem. C*, 2016, **120**, 11716–11726.
45 F. Wang, C. Di Valentin and G. Pacchioni, Semiconductor-to-metal transition in WO 3-x: Nature of the oxygen vacancy, *Phys. Rev. B: Condens. Matter Mater. Phys.*, 2011, **84**, 073103.
46 M. B. Johansson, B. Zietz, G. A. Niklasson and L. Österlund, Optical properties of nanocrystalline WO_3 and WO_{3-x} thin films prepared by DC magnetron sputtering, *J. Appl. Phys.*, 2014, **115**, 213510.
47 S. Z. Karazhanov, Y. Zhang, L. W. Wang, A. Mascarenhas and S. Deb, Resonant defect states and strong lattice relaxation of oxygen vacancies in WO_3, *Phys. Rev. B: Condens. Matter Mater. Phys.*, 2003, **68**, 233204.
48 W. Q. Li, S. Y. Ma, J. Luo, Y. Z. Mao, L. Cheng, D. J. Gengzang, X. L. Xu and S. H. Yan, Synthesis of hollow SnO_2 nanobelts

and their application in acetone sensor, *Mater. Lett.*, 2014, **132**, 338–341.

49 R. Salh, *Defect related luminescence in silicon dioxide network: a review, Crystalline Silicon-Properties and Uses*, 2011, pp. 135–172.

50 H. Zeng, G. Duan, Y. Li, S. Yang, X. Xu and W. Cai, Blue Luminescence of ZnO Nanoparticles Based on Non-Equilibrium Processes: Defect Origins and Emission Controls, *Adv. Funct. Mater.*, 2010, **20**, 561–572.

51 Y. Xia, K. Zhu, Z. Zhang and K. Park, Photo-stimulated desorption of trimethyl acetic acid on cross-linked (1×2) $TiO_2(1\ 1\ 0)$ probed by scanning tunneling microscopy, *Appl. Surf. Sci.*, 2020, **511**, 145553.

52 M. A. Henderson, Photooxidation of Acetone on $TiO_2(110)$: Conversion to Acetate *via* Methyl Radical Ejection, *J. Phys. Chem. B*, 2005, **109**, 12062–12070.

53 O. Tomita, T. Otsubo, M. Higashi, B. Ohtani and R. Abe, Partial Oxidation of Alcohols on Visible-Light-Responsive WO_3 Photocatalysts Loaded with Palladium Oxide Cocatalyst, *ACS Catal.*, 2016, **6**, 1134–1144.

54 A. Rudie, A. M. Schornack, Q. Wu, Q. Zhang and D. Wang, Two-Dimensional Ti_3C_2 MXene-Based Novel Nanocomposites for Breath Sensors for Early Detection of Diabetes Mellitus, *Biosensors*, 2022, **12**, 332.